

Human Brain Imaging and Radiation Dosimetry of ¹¹C-*N-desmethyl-loperamide*, a Positron Emission Tomographic Radiotracer to Measure the Function of P-glycoprotein

Nicholas Seneca^{1*}, Sami S. Zoghbi¹, Jehi-San Liow¹, William Kreisl¹, Peter Herscovitch², Kimberly Jenko¹, Robert L. Gladding¹, Andrew Taku¹, Victor W. Pike¹, and Robert B. Innis¹

¹Molecular Imaging Branch, National Institute of Mental Health, Bethesda, MD, U.S.A.

²PET Department, Clinical Center, National Institutes of Health, Bethesda, MD, U.S.A.

*Address correspondence to:

Nicholas Seneca, PhD

Molecular Imaging Branch

National Institute of Mental Health/National Institutes of Health

31 Center Drive, Room B2B34, MSC 2035

Bethesda, MD 20892-2035, USA

Phone: (301) 435-7846; Fax: (301) 480-3610

E-mail: nicholasseneca@yahoo.com

Running Title: Brain and whole-body imaging of ¹¹C-dLop

Keywords: PET, *N-desmethyl-loperamide*, P-glycoprotein

Number of words in text: 4,763, Figures: 7, Tables: 2

This research was supported by the Intramural Program of NIMH (project #Z01-MH-002852-04).

ABSTRACT

P-glycoprotein (P-gp) is a membrane-bound efflux pump that limits the distribution of drugs to several organs of the body. At the blood-brain barrier, P-gp blocks the entry of both loperamide and its metabolite *N-desmethyl-loperamide* (dLop) and thereby prevents central opiate effects. Animal studies have shown that ^{11}C -dLop, in comparison to ^{11}C -loperamide, is an especially promising radiotracer because it generates negligible radiometabolites that enter brain. The purposes of this study were to determine if ^{11}C -dLop is a substrate for P-gp at the blood-brain barrier in humans and to measure the distribution of radioactivity in the entire body so as to estimate radiation exposure. **Methods:** Brain PET scans were acquired in four healthy subjects for 90 minutes and included concurrent measurements of the plasma concentration of unchanged radiotracer. Time-activity data from whole brain were quantified using a one-tissue compartment model to estimate the rate of entry (K_1) of radiotracer into brain. Whole-body PET scans were acquired in eight healthy subjects for 120 minutes. **Results:** Brain imaging. After injection of ^{11}C -dLop, the concentration of radioactivity in brain was low ($\sim 15\%$ SUV) and stable after ~ 20 minutes. In contrast, uptake of radioactivity in pituitary was about 50-fold higher than that in brain. The plasma concentration of ^{11}C -dLop declined rapidly, but the percentage composition of plasma was unusually stable, with parent radiotracer constituting 85% of total radioactivity after ~ 5 minutes. The rate of brain entry was very low ($K_1 = 0.009 \pm 0.002 \text{ mL}\cdot\text{cm}^{-3}\cdot\text{min}^{-1}$, $n = 4$). Whole-body imaging. As a measure of radiation exposure to the entire body, the effective dose of ^{11}C -dLop was $7.8 \pm 0.6 \text{ }\mu\text{Sv}/\text{MBq}$ ($n = 8$). **Conclusion:** The low brain uptake of radioactivity is consistent with ^{11}C -dLop being a substrate for P-gp in humans and confirms that this

radiotracer generates negligible quantities of brain-penetrant radiometabolites. The low rate of brain entry (K_1) is consistent with P-gp rapidly effluxing substrates while they transit through the lipid bilayer. The radiation exposure of ^{11}C -dLop is similar to that of many other ^{11}C -radiotracers. In conclusion, ^{11}C -dLop is a promising radiotracer to study the function of P-gp at the blood-brain barrier, where impaired function would allow increased uptake into brain.

INTRODUCTION P-glycoprotein (P-gp) is an efflux transporter that is widely distributed in the body and that tends to decrease drug absorption from the intestine, to increase elimination via liver and kidney, and to block distribution to protected tissues such as brain and testes (1). Several radiotracers, usually developed from drugs known to be substrates for P-gp, have been used to image the *in vivo* function of P-gp (2-9). Sestamibi was the first radiotracer used to image P-gp function (8) and was labeled with ^{99m}Tc for SPECT and ^{94m}Tc for PET. In addition to measuring the over expression of P-gp in multidrug resistance cancer, $^{99m/94m}\text{Tc}$ -sestamibi is useful to measure the function of P-gp at the blood-brain barrier, as demonstrated in P-gp knock out mice. Because of the high energy emissions of ^{94m}Tc and the subsequent decay of daughter radionuclides, other radiotracers were developed for PET and labeled with ^{11}C or ^{18}F . These radiotracers, including ^{11}C -loperamide, ^{11}C -verapamil, and ^{18}F -paclitaxel, generate brain-penetrant radiometabolites which obscure the chemical source of the radioactive emissions from the brain.

Loperamide is used to treat diarrhea and acts on μ opiate receptors in the intestine. Loperamide has virtually no central opiate effects, because P-gp avidly blocks its entry into brain. Following reports from others (7, 10, 11), we studied both ^{11}C -loperamide and ^{11}C -dLop in mice and monkeys as measures of P-gp function (4, 9, 12). As expected, both radioligands were avid substrates and had high brain uptake after inactivation of P-gp by either genetic knockout or pharmacological inhibition. However, injection of ^{11}C -loperamide led to the accumulation of significant concentrations of radiometabolites, including ^{11}C -dLop, in brain. In contrast, injection of ^{11}C -dLop itself markedly reduced radiometabolites in brain.

In summary, our animal studies showed that ^{11}C -dLop fulfills the two primary requirements for a radiotracer to measure P-gp function at the blood-brain barrier. That is, brain uptake is high after P-gp blockade, and the vast majority of radioactivity in brain reflects that of the parent radiotracer. The purposes of this study were to determine if ^{11}C -dLop is a substrate for P-gp at the blood-brain barrier in humans and to measure the distribution of radioactivity in the entire body so as to estimate radiation exposure.

MATERIALS AND METHODS

Radiotracer preparation

^{11}C -dLop was prepared by methylation of the primary amide precursor with ^{11}C -iodomethane (4). Preparations were conducted according to our Investigational New Drug Application #101,092, submitted to the US Food and Drug Administration, and a copy of which is available at: <http://pdsp.med.unc.edu/snidd/>. The radiotracer was obtained in high radiochemical purity (100%) and with specific activity at time of injection of 93 ± 31 GBq/ μmol ($n = 12$ batches).

Human subjects

Twelve healthy volunteers participated: 8 females and 4 males, 26 ± 3 years of age, 69 ± 13 kg body weight. All subjects were free of current medical and psychiatric illness based on history, physical examination, electrocardiogram, urinalysis including drug screening, and blood tests. The subjects' vital signs were recorded before ^{11}C -dLop injection and at 15, 30, and 60 or 90 minutes after injection. Approximately 24 h after the PET scan, subjects returned to repeat urinalysis and blood tests.

PET imaging

Brain imaging

After injection of ^{11}C -dLop (730 ± 16 MBq) in four subjects, PET scans were acquired for 60 ($n = 2$) or 90 ($n = 2$) minutes in 21 or 27 frames, respectively. PET scans were acquired in 3D mode with the High Resolution Research Tomograph (Siemens/CPS, Knoxville, TN, USA). Before radiotracer injection, a six-minute transmission scan was collected using a ^{137}Cs point source for attenuation correction.

Whole-body imaging

After injection of ^{11}C -dLop (744 ± 5 MBq) in eight subjects, whole-body PET scans were acquired in 2D mode on seven segments of 15 cm each, from the head to upper thigh using a GE Advance tomograph (GE Healthcare, Waukesha, WI). The total scanning time was ~120 minutes, with frames of 4×15 s, 3×30 s, 3×1 minute, 3×2 minutes, and 1×4 minutes for each of the seven body sections. Before radiotracer injection, a 32-minute transmission scan of the seven segments of the body was collected using a ^{68}Ge rod source for attenuation correction.

Measurement of ^{11}C -dLop in plasma

Blood samples (1.5 mL each) were drawn from the radial artery at 15 s intervals until 120 s, followed by samples at 3, 5, and 10 minutes, and 3 mL samples at 20 and 30 minutes, and 4.5 mL samples at 45, 60, 75, and 90 minutes. The plasma time-activity curve was corrected for the fraction of unchanged radiotracer, as previously described (13). The free fraction of ^{11}C -dLop in plasma was measured by ultrafiltration through Centrifree membrane filters, as previously described (14).

Image analysis and calculation of outcome measures

Brain imaging

PET and MRI images were coregistered using Statistical Parametric Mapping 2 (SPM 2; Wellcome Department of Cognitive Neurology, London, UK). PET images of the entire scanning session were summed together to more clearly delineate brain and venous sinuses. Five regions of interest encompassing the entire brain, the pituitary gland, the venous sinuses, the fourth ventricle and the choroid plexus were drawn on the coregistered MRI and mapped onto the PET images. Time-activity curves were expressed as percentage standardized uptake value (%SUV), which normalizes for injected activity

and body weight: $(\% \text{ injected activity/cm}^3 \text{ tissue}) \times (\text{g body weight})$. Image and kinetic analyses were performed using PMOD 2.85 (pixel-wise modeling software; PMOD Technologies Ltd., Zurich, Switzerland).

Time-activity data were analyzed with one- and two-tissue compartment models, using the radiometabolite-corrected plasma input function. To correct the brain data for its vascular component, radioactivity in serial whole blood was measured and then subtracted from the PET measurements assuming that cerebral blood volume is 5% of total brain volume.

Whole-body imaging

Whole body tomographic PET images were compressed into a single planar image, and regions of interest were drawn on source organs that could be identified: thyroid, brain, heart, liver, lungs, kidneys, spleen, lumbar vertebrae and urinary bladder. The lumbar vertebrae were used as an approximation for uptake in the red marrow, since they contain ~12.3% of the red marrow in an adult (15).

At each time point, activities of identifiable source organs were converted into the fraction of the total injected activity. The area under the curve of each organ was calculated by the trapezoidal method to the end of imaging (~ 120 minutes). The area after the last time point to infinity was calculated by assuming that further decline occurred by only physical decay, without any biological clearance. The area under the curve of % injected activity from time zero to infinity is equal to residence time of the organ.

The mean total radioactivity in urinary bladder was fitted with an exponential curve to estimate the percentage of injected activity excreted via this route. The dynamic

bladder model with 2.4 h voiding interval was implemented in OLINDA/EXM version 1.0 to calculate organ absorbed doses (16).

The organ values of injected activity were corrected for recovery of measured activity. To accomplish this, a large region of interest was placed over the entire body for each of the 14 frames. The injected activity of each source organ at every time point was corrected for recovery by multiplying by $100/X$, where X is the measured recovery for the individual frame. The average recovery of all frames in eight subjects was $\sim 92\%$. If no radioactivity is lost to excretion, the total of all residence times equals $T_{1/2}/\ln(2)$, where $T_{1/2} = 20.4$ minutes = 0.34 h, and $T_{1/2}/\ln(2) = 0.49$ h. The residence time of “remainder of body” for each subject was calculated as 0.49 h minus the sum of the residence times of the source organs.

Group data are expressed as mean \pm SD.

RESULTS

Minimal brain uptake of ^{11}C -dLop

Following injection of ^{11}C -dLop, uptake of radioactivity in the whole brain, including its vascular component, was low (<50% SUV; Fig. 1 and 2A). Uptake in brain tissue itself, corrected for blood radioactivity, achieved concentrations of only ~15% SUV by 15–20 minutes and was stable until the end of the scanning session (60 minutes in two subjects and 90 minutes in the other two subjects). This low uptake of ~15% SUV in brain from the four subjects who had dedicated brain imaging was confirmed in the eight subjects who had whole body imaging (Fig. 2B). In contrast to the low uptake in brain, pituitary and choroid plexus accumulated high concentrations of radioactivity about 650% and 280% SUV, respectively (Fig. 3). Similar to brain, uptake in the pituitary and choroid plexus was relatively rapid and stable until the end of the scanning session (90 minutes). Because of the limited resolution of the PET images, we could not further discern whether the uptake was in anterior pituitary (inside the blood brain barrier) and/or posterior pituitary (outside the blood brain barrier).

Uptake in the choroid plexus and venous sinus were visible on the tomographic images (Fig. 1) but were even more apparent in rotating three-dimensional images of the brain acquired during the first 10 minutes (Supplemental Fig. 1).

To determine whether uptake in the choroid plexus was subsequently excreted into the CSF, we compared the time course of radioactivity in these two regions. In fact, activity accumulated in choroid plexus (i.e., increased from zero activity to a stable plateau of about 280% SUV) – whereas activity in the CSF of the fourth ventricle declined from an early peak to a low stable level of about 10% SUV. Thus, uptake in the

choroid plexus appeared to be trapped in this tissue and showed no evidence of excretion into the CSF.

Overall, radioactivity in regions within the skull reflected two general sources: blood pool (whole brain; venous sinus) and accumulation in tissues (brain itself, pituitary, and choroid plexus). Of course, the time course of radioactivity in the blood pool reflected that in plasma – namely, a rapid peak, followed by a rapid decline. Thus, whole brain and venous sinus had an early peak followed by a rapid washout. In contrast, brain itself, pituitary, and choroid plexus increased to a plateau. However, radioactivity in all five regions (whole brain, brain corrected for vascular component, venous sinus, pituitary, and choroid plexus) were relatively stable for the terminal portion of the scan.

Plasma clearance

The average concentration of ^{11}C -dLop in plasma peaked at ~ 1 minute and decreased rapidly in four subjects (Fig. 4). The concentrations after this peak were fitted well with a biexponential function and had mean half lives of 0.4 and 15 minutes. Calculated as the partial areas under the concentration *vs.* time curve, these two half-lives accounted for 40% and 60% of the total area under the curve from peak to infinity.

The fraction of ^{11}C -dLop, expressed as a percentage of total plasma activity, composed a stable and high percentage (85%) of total radioactivity from 5 minutes to the end of the scan (Fig. 5A). Five radiometabolite peaks were detected in arterial plasma samples with high-performance liquid chromatography (Fig. 5B). All five radiometabolite peaks earlier than the parent radiotracer and were therefore less lipophilic than dLop. The plasma free fraction of ^{11}C -dLop was $11.4 \pm 3.3\%$ in four subjects.

Kinetic analysis

Compartmental modeling of whole brain time-activity data and serial concentrations of plasma ^{11}C -dLop were poorly fit by a one-tissue compartment model and did not converge with a two-tissue compartment model. For the one-tissue compartment model, K_1 was poorly identified ($\sim 30\%$), and k_2 was essentially not identified ($> 1,000\%$). As expected from the low brain uptake, the rate constant K_1 was only $0.009 \pm 0.002 \text{ mL}\cdot\text{cm}^{-3}\cdot\text{min}^{-1}$ (mean \pm SD in four subjects). Since the stable uptake in brain suggested an irreversible process, we also fitted brain data with k_2 set to 0. This constraint insignificantly affected the value of K_1 .

Whole-body biodistribution

Lungs, liver, spleen, thyroid, urinary bladder, and kidneys were easily identified as source organs on the whole body images (Fig. 6). Lungs had the highest uptake of radioactivity, with peak value of 33% at ~ 2 minutes (Fig. 7). The liver also exhibited high uptake, which continuously increased over the duration of scan to 22% injected activity at ~ 100 minutes (Fig. 7A). Uptake in liver increased ~ 1.5 -fold from 20 minutes until the end of scan. Uptake in brain peaked quickly and leveled off at 0.03% injected activity from 3 minutes until the end of scan (Fig. 7B). The mean cumulative urine activity was well fitted ($r^2 = 0.92$) with an exponential curve (data not shown). The exponential fitting had an asymptote of $\sim 4\%$ of injected activity at time of infinity, indicating that only $\sim 4\%$ injected activity was excreted by the urinary route. Please note that the whole body images in Fig. 6 use a format (maximal intensity projection) that emphasizes anatomy with high radioactivity uptake but may cause visual misperception of the total radioactivity – *e.g.*, in urinary bladder. Although difficult to visualize on the maximal intensity projection images (Fig. 6), the horizontal and mid-sagittal sinuses were

easily seen on rotating 3-dimensional images at early times (0 – 10 minutes) after injection of ^{11}C -dLop (Supplemental Fig. 1).

Human residence times were estimated using average values from the planar images (Table 1). The organs with the highest radiation burden ($\mu\text{Sv}/\text{MBq}$) were kidneys (50.1), spleen (30.5), and lungs (27.0) (Table 2). With a 2.4-h voiding interval, the effective dose was $7.8 \pm 0.6 \mu\text{Sv}/\text{MBq}$ ($28.7 \pm 2.2 \text{ mrem}/\text{mCi}$; mean \pm SD in eight subjects).

DISCUSSION

We found that ^{11}C -dLop has minimal uptake in healthy human brain. The low brain uptake of radioactivity ($\sim 15\%$ SUV) confirms that minimal amounts of radiometabolites (and parent radiotracer) enter brain. The low rate of brain entry ($K_1 = 0.009 \text{ mL}\cdot\text{cm}^{-3}\cdot\text{min}^{-1}$) is consistent with ^{11}C -dLop being a substrate for P-gp, which blocks entry of compounds rather than enhances removal. As a measure of radiation exposure to the entire body, the effective dose of ^{11}C -dLop was $7.8 \pm 0.6 \mu\text{Sv}/\text{MBq}$. The mass dose of carrier *N-desmethyl-loperamide* ($4.1 \pm 1.5 \mu\text{g}$) injected with ^{11}C -dLop produced no subjective effects and no significant changes in laboratory tests, EKG, blood pressure, pulse, or respiration rate. Therefore, ^{11}C -dLop appears safe from both pharmacological and radiological perspectives.

Comparison with ^{11}C -verapamil

^{11}C -Verapamil is the radiotracer that has been most extensively studied as an agent for measuring P-gp function at the blood-brain barrier. ^{11}C -Verapamil generates more brain-penetrant radiometabolites than ^{11}C -dLop in rats and possibly also in humans. At 30 minutes after injection in rats, $\sim 30\%$ of brain radioactivity is caused by radiometabolites for ^{11}C -verapamil (17), compared to $< 10\%$ for ^{11}C -dLop (4). ^{11}C -Verapamil likely generates radiometabolites in humans, as suggested by 4-fold higher brain uptake in healthy subjects of ^{11}C -verapamil than of ^{11}C -dLop: 70% vs. 15% SUV, respectively (18). Consistent with its greater brain uptake, the K_1 of ^{11}C -verapamil ($0.05 \text{ mL}\cdot\text{cm}^{-3}\cdot\text{min}^{-1}$) is about five-fold greater than that of ^{11}C -dLop ($0.009 \text{ mL}\cdot\text{cm}^{-3}\cdot\text{min}^{-1}$).

The metabolism of ^{11}C -dLop in humans had one unexpected finding – namely, ^{11}C -dLop composed a stable and high percentage (85%) of total radioactivity from 5

minutes to the end of the scan. Our prior study of ^{11}C -dLop in monkey showed the more typical pattern in which the percentage composition of parent radiotracer declines over time. The percentage of radioactivity that was ^{11}C -dLop in monkey plasma declined from 100% at time 0 to 50% at 40 minutes (4). The high percentage composition of human plasma by ^{11}C -dLop may help ensure that few radiometabolites enter brain. Furthermore, the radiometabolites in both human and monkey plasma eluted earlier than the parent radiotracer and were, therefore, less lipophilic than dLop (Fig. 5B). In fact, the major radiometabolite (A) was the least lipophilic (Fig. 5B) and, therefore, the least likely to enter brain.

Radiation dosimetry and whole-body imaging

The radiation exposure of ^{11}C -dlop (7.8 $\mu\text{Sv}/\text{MBq}$) was similar to that of many other ^{11}C -radiotracers (range of $\sim 4.3 - 14.1 \mu\text{Sv}/\text{MBq}$) and was, therefore, an expected finding (19). After injection of ^{11}C -dLop, both thyroid and pituitary had high uptake of radioactivity in humans (current study) and in monkeys (4, 12). The dosimetry software (OLINDA-EXM) calculates exposure to the thyroid but not to the pituitary (Table 2). To estimate exposure to the pituitary, we assumed that its concentration of radioactivity was constant at 650% SUV (Fig 2) and that its weight was 0.6 g. Considering the pituitary to be a small sphere such that the dose to the organ is only from activity in the organ itself, the pituitary dose was 12.4 μSv per MBq injected activity. This value would be an overestimation if the radioactivity derives from a volume larger than the pituitary itself, which we cannot determine with the resolution of the PET scans. Nevertheless, this estimated radiation exposure to the pituitary is similar to that of the liver (12.9 $\mu\text{Sv}/\text{MBq}$),

but much less than that of the kidney (50.1 $\mu\text{Sv}/\text{MBq}$), which had the highest radiation exposure.

Another surprising finding was the prominent visualization of the system of venous sinuses surrounding the brain. Although difficult to discern on the coronal images (Fig. 6), the horizontal and mid-sagittal sinuses were easily seen on sagittal or rotating three-dimensional images at early times (0-10 minutes) after injection of the radiotracer (Supplemental Fig 1). The sinuses were easily visualized because the adjacent brain had negligible radioactivity.

Finally, in this study we estimated radiation dosimetry exposure using 2-D planar images which have been found to provide conservative estimates of radiation exposure. We previously compared radiation exposure estimated with 2-D planar, bisected and thin-slice tomographic images using the phosphodiesterase 4 radiotracer ^{11}C -(*R*)-rolipram and substance P (NK_1) receptor radiotracer ^{18}F -SPA-RQ (20, 21). In both studies, planar and bisected images provided organ dose estimates similar to, but slightly higher than, those of thin-slice images.

CONCLUSION

The low uptake of radioactivity in brain is consistent with ^{11}C -dLop being a substrate for P-gp in humans and confirms that this radiotracer generates negligible quantities of brain-penetrant radiometabolites. The low rate of brain entry (K_1) is consistent with P-gp rapidly effluxing substrates while they transit through the lipid bilayer. The radiation exposure of ^{11}C -dLop is similar to that of many other ^{11}C -radiotracers and would allow multiple PET scans per year in the same subject. In conclusion, ^{11}C -dLop is a promising radiotracer to study the function of P-gp at the

blood-brain barrier, where impaired function would allow increased uptake into brain.

ACKNOWLEDGEMENTS

The Intramural Research Program of NIMH supported this research (project # Z01-MH-002852-04). We thank the staff of the NIH PET Department for successfully performing the PET studies; Edward Tuan for assistance with the blood samples; Maria Ferraris Araneta CRNP for subject recruitment and care; and PMOD Technologies (Zurich, Switzerland) for providing its image analysis and modeling software. A patent application has been filed on behalf of the US government for PET imaging of P-gp function; Drs. Zoghbi, Pike, and Innis could personally benefit from this patent.

Figure legends

Figure 1. PET images of ^{11}C -dLop in human brain and corresponding MRI. PET images (left column) were summed from 0 to 90 min and pixel values represent mean concentration of radioactivity (%SUV). Coregistered MRI images are on right column, and the fused PET and MRI images are in the middle column. Arrows point to choroid plexus on the medial surfaces of the lateral ventricles and on the roof of the third and fourth ventricles.

Figure 2. (A) Concentration of radioactivity in brain, with (\square) and without (\blacksquare) vascular correction, in four subjects who had head-dedicated imaging. Symbols represent mean values. SD bars are included for all points after 18 minutes. Note that the SD bars are smaller than the symbols for all points after 60 minutes. (B) Concentration of radioactivity in brain in eight subjects who had whole-body imaging. Vascular correction of brain activity could not be performed in these subjects, since no blood was collected during scanning.

Figure 3. After injection of ^{11}C -dLop, radioactivity in the pituitary gland (\circ) and choroid plexus (\blacksquare) peaked quickly and remained stable during the course of the scan. Whereas the uptake in the venous sinus (Δ) and fourth ventricle (i.e., CSF; (\blacktriangledown)) peaked quickly and stabilized at a lower level. Symbols represent mean values in four subjects. For clarity, SD bars are included only after 5 minutes and for every other time point.

Figure 4. Concentration of unchanged ^{11}C -dLop in plasma after radiotracer injection. The curve is shown with two time intervals (0 to 5 and 5 to 90 minutes) because of high concentrations at early time points.

Figure 5. (A) The percentage composition of plasma radioactivity over time is shown for ^{11}C -dLop (■) and total radiometabolites (○) ($n = 4$ subjects). Symbols represent the mean \pm SD, although the SD is sometimes smaller than the size of the symbol. (B)

Representative radiochromatogram of plasma at 30 minutes after injection of ^{11}C -dLop. Parent constituted 88% of total radioactivity. Radiometabolites (A–E) are less lipophilic than ^{11}C -dLop.

Figure 6. Maximal intensity projection images of the distribution of radioactivity in a healthy male subject at 3, 20, and 100 minutes after injection of ^{11}C -dLop.

Figure 7. Uptake of radioactivity in organs that could be visually identified on planar whole-body images. The organ's activity is expressed as a percentage of the injected activity. Data represent mean \pm SD in eight subjects.

Supplemental Figure 1. Images from 0 to 10 minutes were summed and displayed as a rotating object. Radioactivity in the venous sinuses reflects the blood pool and derives largely from early times (0-3 minutes). Radioactivity in the choroid plexus of the lateral ventricles and in pituitary represents accumulation in tissue and derives largely from later portions (3 – 10 minutes) of this time interval.

Table 1. Residence times of source organs.

Source Organ	Residence time (h)
Thyroid	0.001 ± 0.000
Brain	0.002 ± 0.001
Lungs	0.102 ± 0.014
Liver	0.068 ± 0.017
Urinary bladder	0.013 ± 0.005
Spleen	0.019 ± 0.005
Kidneys	0.055 ± 0.007
Red marrow	0.009 ± 0.003
Remainder in body	0.220 ± 0.007

Data represent mean ± SD.

Table 2. Radiation dosimetry estimates for ^{11}C -dLop determined from eight healthy subjects.

Target Organ Doses	$\mu\text{Sv/MBq}$	mrem/mCi
Adrenals	4.2 ± 0.1	15.4 ± 0.4
Brain	0.8 ± 0.2	2.9 ± 0.7
Breasts	2.0 ± 0.1	7.5 ± 0.2
Gallbladder wall	3.8 ± 0.3	14.1 ± 1.1
LLI wall	1.9 ± 0.1	7.2 ± 0.4
Small intestine	2.3 ± 0.1	8.5 ± 0.2
Stomach	2.8 ± 0.1	10.3 ± 0.3
ULI wall	2.3 ± 0.1	8.7 ± 0.3
Heart wall	3.2 ± 0.1	11.8 ± 0.3
Kidneys	50.1 ± 6.0	184.9 ± 22
Liver	12.9 ± 2.7	47.9 ± 10
Lungs	27.0 ± 3.4	99.8 ± 13
Muscle	2.0 ± 0.0	7.3 ± 0.1
Ovaries	2.0 ± 0.1	7.5 ± 0.4
Pancreas	4.0 ± 0.2	14.9 ± 0.6
Red marrow	2.9 ± 0.3	10.9 ± 1.1
Osteogenic cells	3.0 ± 0.2	11.2 ± 0.7
Skin	1.4 ± 0.0	5.3 ± 0.1
Spleen	30.5 ± 6.8	112.7 ± 25
Testes	1.5 ± 0.1	5.5 ± 0.3
Thymus	2.3 ± 0.1	8.6 ± 0.3
Thyroid	14.7 ± 6.2	54.5 ± 23
Urinary bladder wall	10.8 ± 3.3	39.8 ± 12
Uterus	2.2 ± 0.2	8.3 ± 0.7
Total body	2.9 ± 0.0	10.8 ± 0.1
Effective dose	7.8 ± 0.6	28.7 ± 2.2

Data represent mean \pm SD.

REFERENCES

1. Fromm MF. Importance of P-glycoprotein at blood-tissue barriers. *Trends Pharmacol Sci*. 2004;25:423-429.
2. Bigott HM, Prior JL, Piwnica-Worms DR, Welch MJ. Imaging multidrug resistance P-glycoprotein transport function using microPET with technetium-94m-sestamibi. *Mol Imaging*. 2005;4:30-39.
3. Kurdziel KA, Kiesewetter DO, Carson RE, Eckelman WC, Herscovitch P. Biodistribution, radiation dose estimates, and in vivo Pgp modulation studies of ^{18}F -paclitaxel in nonhuman primates. *J Nucl Med*. 2003;44:1330-1339.
4. Lazarova N, Zoghbi S, Jinsoo H, et al. Synthesis and evaluation of *N*-methyl- ^{11}C -*N*-Desmethyl-loperamide as a new and improved PET radiotracer for Imaging P-gp function. *J Med Chem*. 2008;in revision.
5. Lee YJ, Maeda J, Kusahara H, et al. In vivo evaluation of P-glycoprotein function at the blood-brain barrier in nonhuman primates using [^{11}C]verapamil. *J Pharmacol Exp Ther*. 2006;316:647-653.
6. Lubberink M, Luurtsema G, van Berckel BN, et al. Evaluation of tracer kinetic models for quantification of P-glycoprotein function using (*R*)-[^{11}C]verapamil and PET. *J Cereb Blood Flow Metab*. 2007;27:424-433.
7. Passchier R, Comley R, Salinas C. The role of P-glycoprotein on blood brain barrier permeability of ^{11}C -Loperamide in humans. *Neuroimage*. 2008;41:P131.
8. Piwnica-Worms D, Chiu ML, Budding M, Kronauge JF, Kramer RA, Croop JM. Functional imaging of multidrug-resistant P-glycoprotein with an organotechnetium complex. *Cancer Res*. 1993;53:977-984.
9. Zoghbi SS, Liow JS, Yasuno F, et al. ^{11}C -loperamide and its *N*-desmethyl radiometabolite are avid substrates for brain permeability-glycoprotein efflux. *J Nucl Med*. 2008;49:649-656.
10. Passchier J, Bender D, Matthews JC, Lawrie KW, Gee AD. ^{11}C -Loperamide: A novel and sensitive PET probe for quantification of changes in P-glycoprotein functionality [Abstract]. *Mol Imaging Biol*. 2003;5:121.
11. Wilson A, Passchier J, Garcia A. Production of the P-glycoprotein marker, ^{11}C -Loperamide, in clinically useful quantities. *J Label Compd Radiopharm*. 48:S142.
12. Liow JS, Kreisl W, Zoghbi SS, et al. P-Glycoprotein Function at the Blood-Brain Barrier Imaged Using ^{11}C -*N*-Desmethyl-Loperamide in Monkeys. *J Nucl Med*. 2009;50:108-115.

13. Zoghbi SS, Shetty UH, Ichise M, et al. PET Imaging of the dopamine transporter with ^{18}F -FECNT: A polar radiometabolite confounds brain radioligand measurements. *J Nucl Med.* 2006;47:520-527.
14. Gandelman MS, Baldwin RM, Zoghbi SS, Zea-Ponce Y, Innis RB. Evaluation of ultrafiltration for the free-fraction determination of single photon emission computed tomography (SPECT) radiotracers: beta-CIT, IBF, and iomazenil. *J Pharm Sci.* 1994;83:1014-1019.
15. Valentin J. Basic Anatomical and Physiological Data for Use in Radiological Protection: Reference Values. ICRP Publication 89. *Pergamon Press.* 2001;167-185.
16. Stabin MG, Sparks RB, Crowe E. OLINDA/EXM: the second-generation personal computer software for internal dose assessment in nuclear medicine. *J Nucl Med.* 2005;46:1023-1027.
17. Luurtsema G, Molthoff CF, Schuit RC, Windhorst AD, Lammertsma AA, Franssen EJ. Evaluation of (*R*)- ^{11}C -verapamil as PET tracer of P-glycoprotein function in the blood-brain barrier: kinetics and metabolism in the rat. *Nucl Med Biol.* 2005;32:87-93.
18. Ikoma Y, Takano A, Ito H, et al. Quantitative analysis of ^{11}C -verapamil transfer at the human blood-brain barrier for evaluation of P-glycoprotein function. *J Nucl Med.* 2006;47:1531-1537.
19. Brown AK, Fujita M, Fujimura Y, et al. Radiation dosimetry and biodistribution in monkey and man of ^{11}C -PBR28: a PET radioligand to image inflammation. *J Nucl Med.* 2007;48:2072-2079.
20. Sprague DR, Chin FT, Liow JS, et al. Human biodistribution and radiation dosimetry of the tachykinin NK1 antagonist radioligand [^{18}F]SPA-RQ: comparison of thin-slice, bisected, and 2-dimensional planar image analysis. *J Nucl Med.* 2007;48:100-107.
21. Sprague DR, Fujita M, Ryu YH, Liow JS, Pike VW, Innis RB. Whole-body biodistribution and radiation dosimetry in monkeys and humans of the phosphodiesterase 4 radioligand [^{11}C]-(*R*)-rolipram: comparison of two-dimensional planar, bisected and quadrisectioned image analyses. *Nucl Med Biol.* 2008;35:493-500.

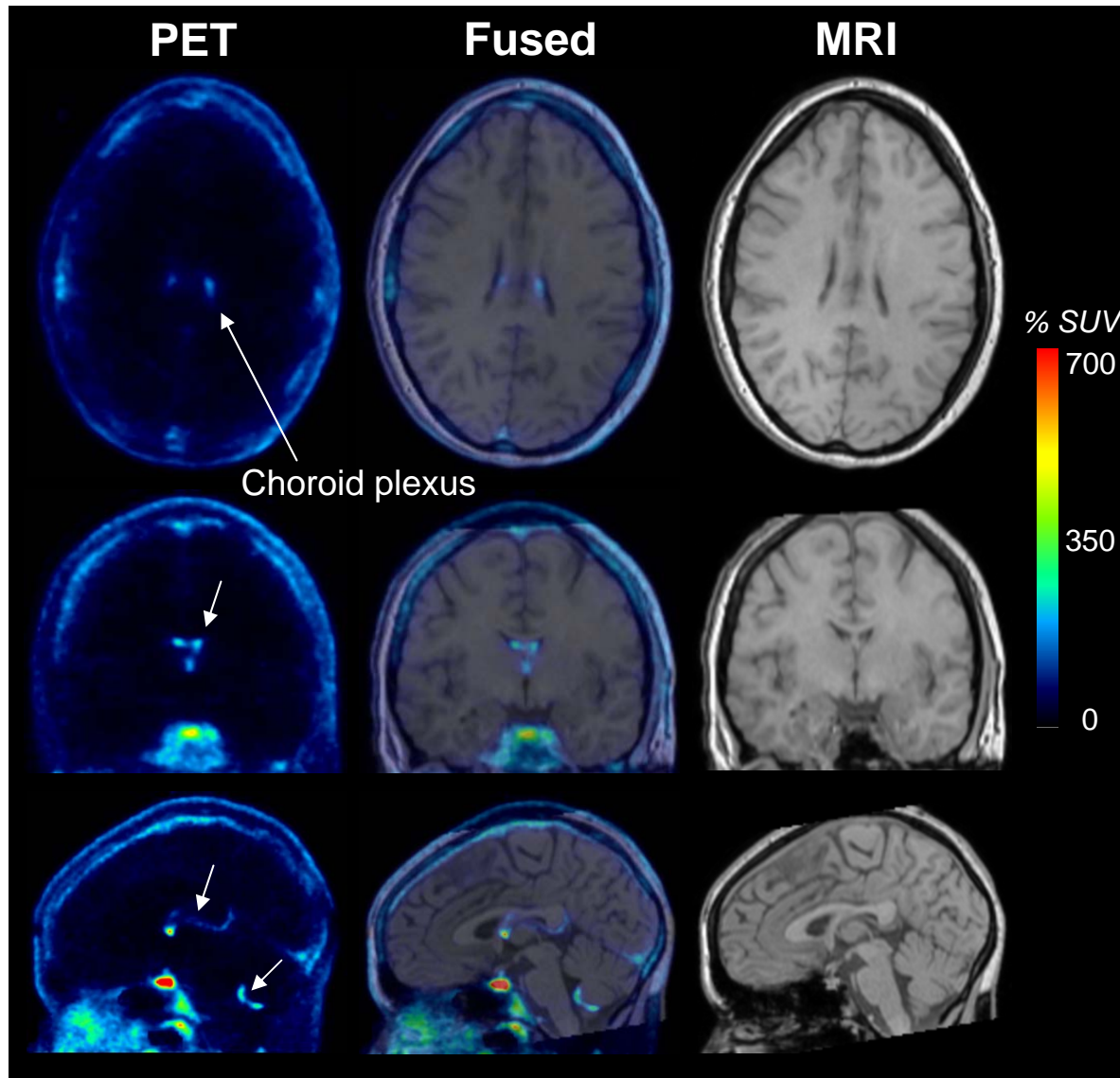


Figure 1.

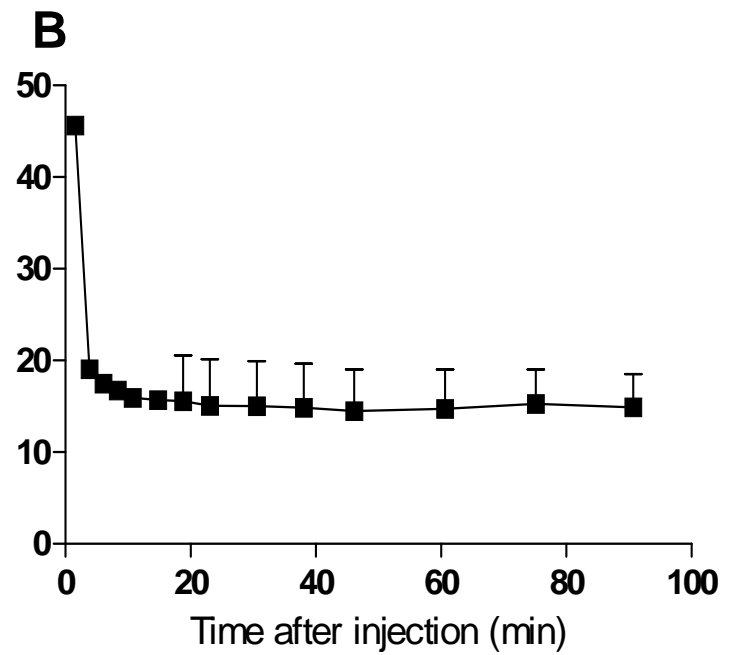
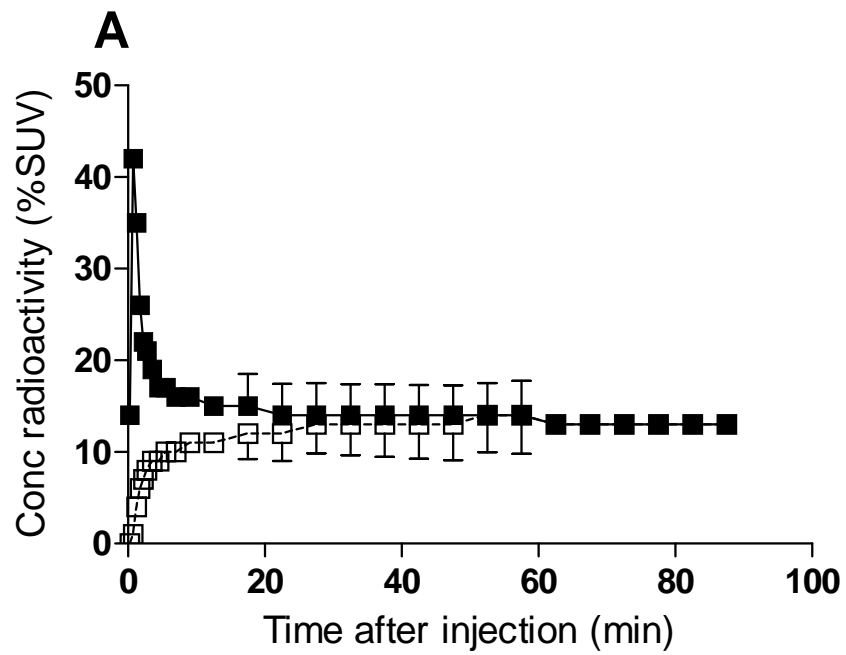


Figure 2.

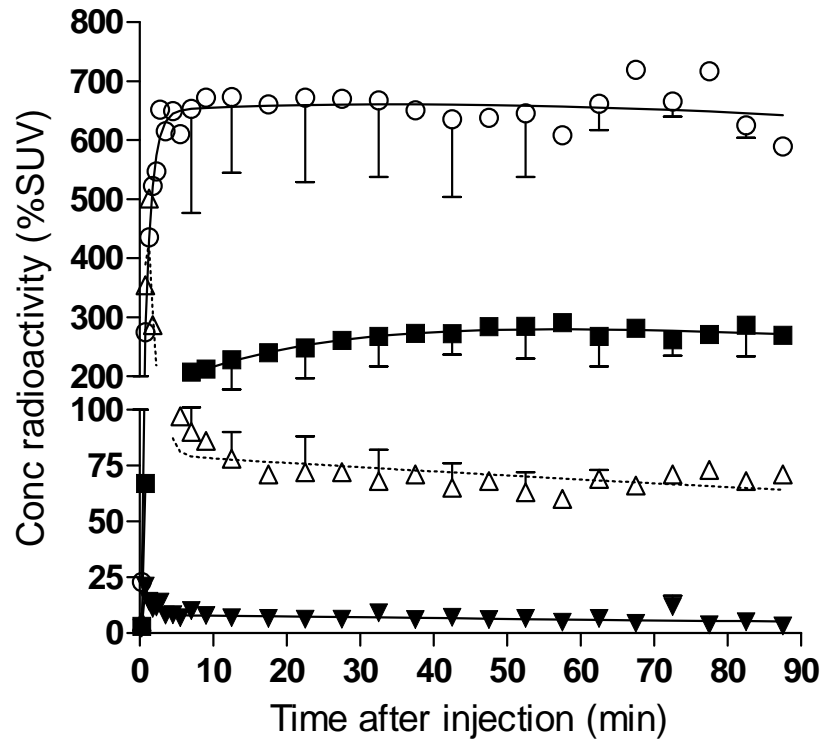


Figure 3.

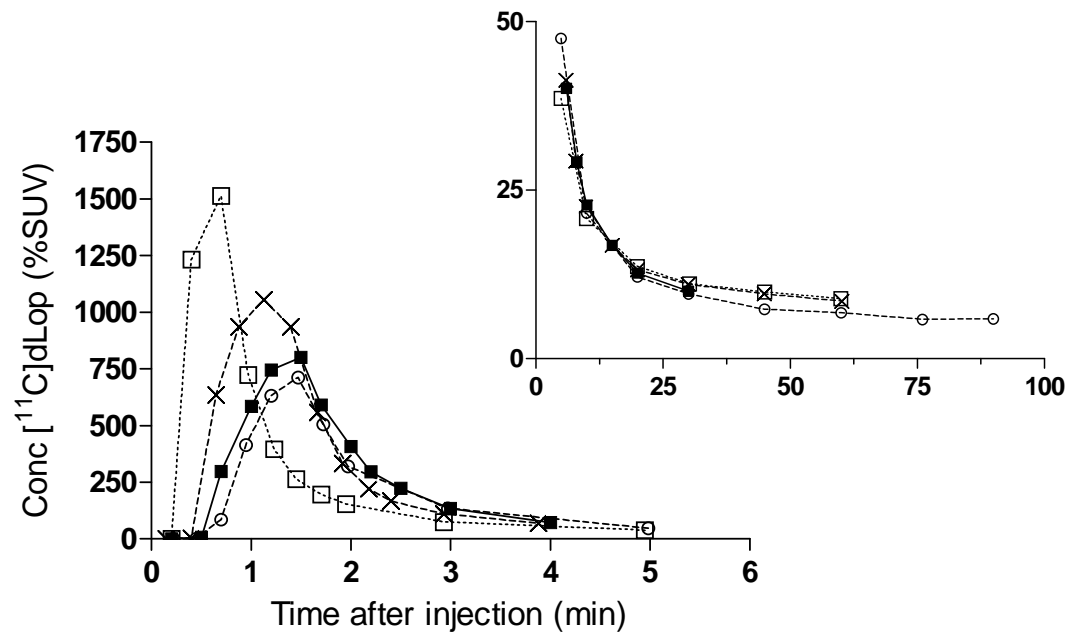


Figure 4.

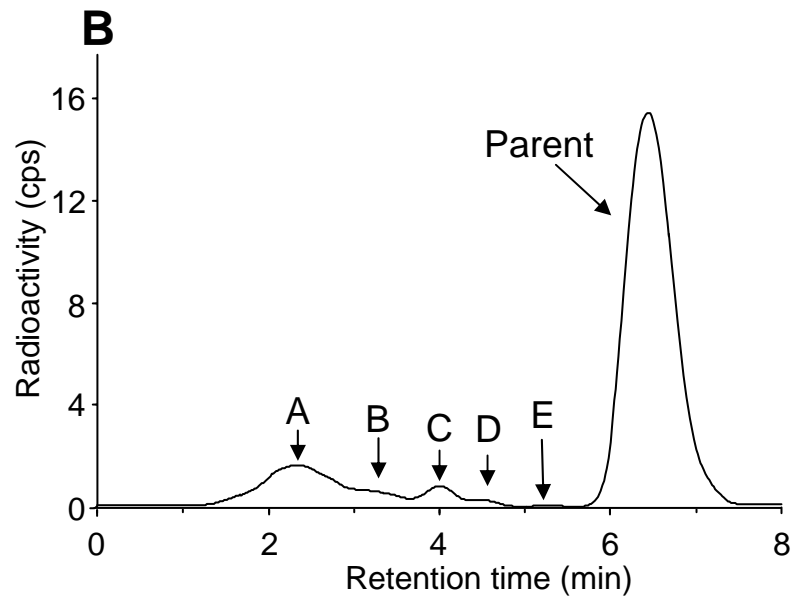
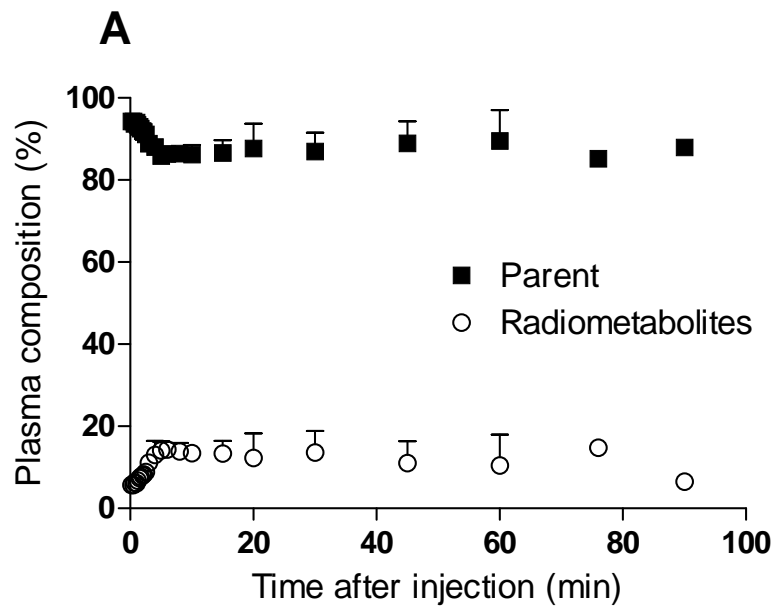


Figure 5.

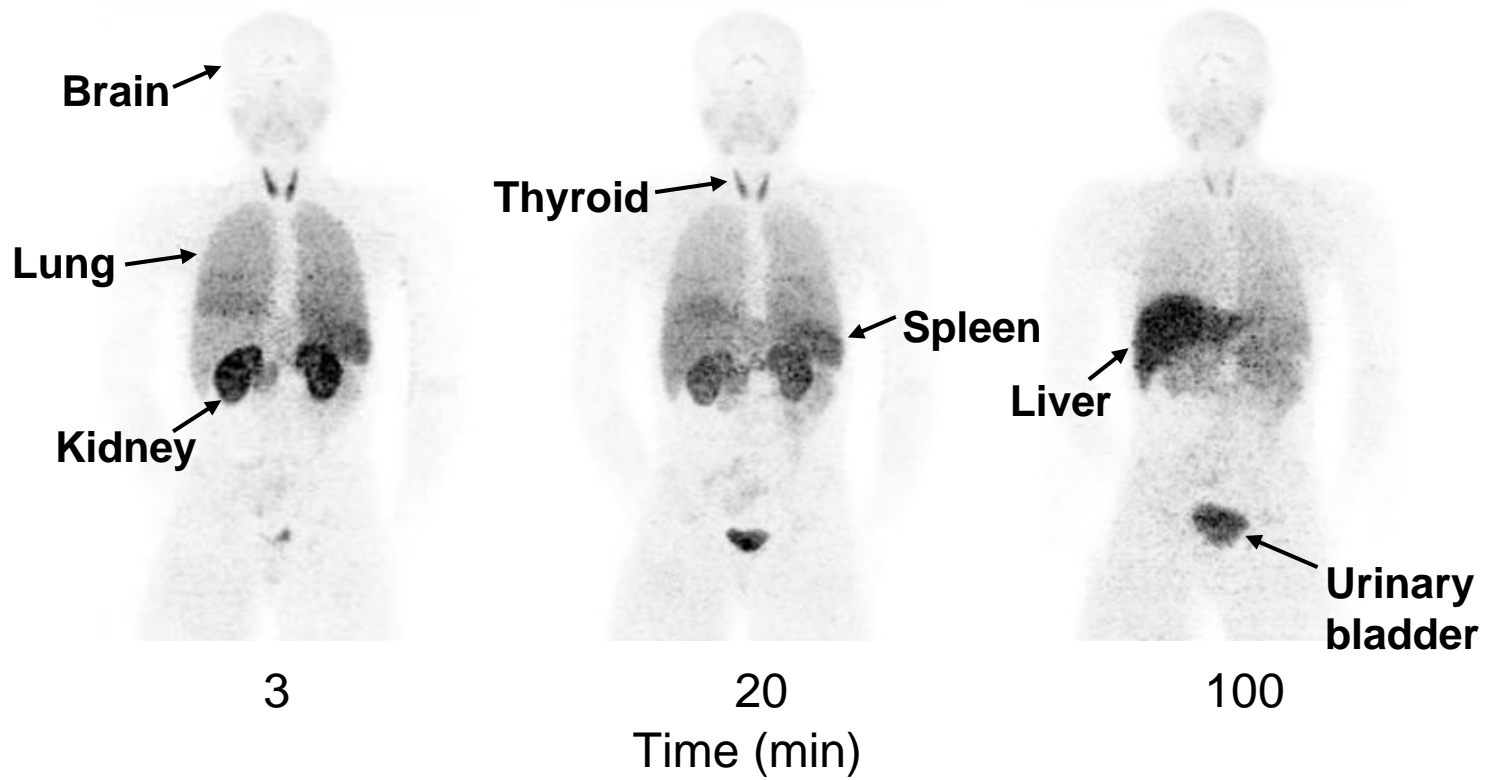


Figure 6.

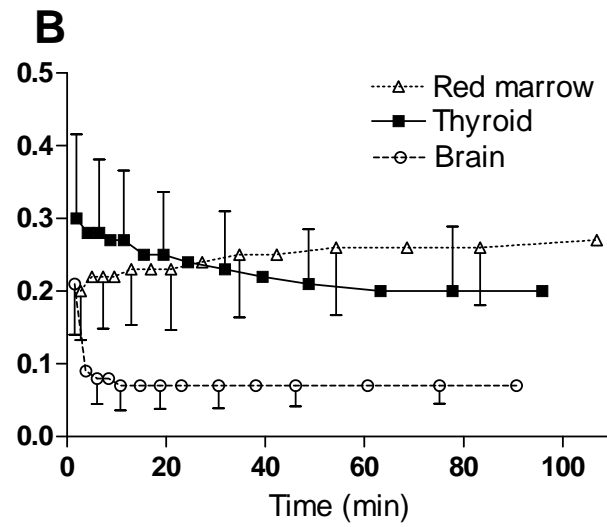
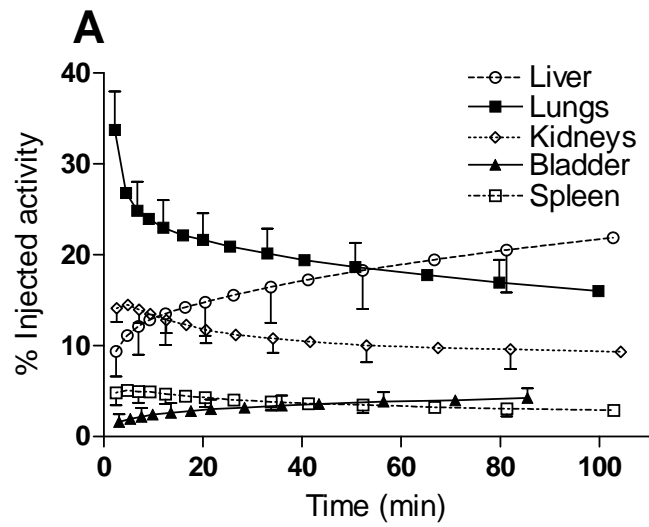


Figure 7.